OCEAN PLANKTON

Environmental characteristics of Agulhas rings affect interocean plankton transport

Emilie Villar,[1]* Gregory K. Farrant,[2,3]† Michael Follows,[11]† Laurence Garczarek,[2,3]† Sabrina Speich,[5,23]¶ Stéphane Audic,[2,3] Lucie Bittner,[2,3,4]‡ Bruno Blanke,[5] Jennifer R. Brum,[6]** Christophe Brunet,[7] Raffaella Casotti,[7] Alison Chase,[8] John R. Dolan,[9,10] Fabrizio d'Ortenzio,[9,10] Jean-Pierre Gattuso,[9,10] Nicolas Grima,[5] Lionel Guidi,[9,10] Christopher N. Hill,[11] Oliver Jahn,[11] Jean-Louis Jamet,[12] Hervé Le Goff,[13] Cyrille Lepoivre,[1] Shruti Malviya,[4] Eric Pelletier,[14,15,16] Jean-Baptiste Romagnan,[9,10] Simon Roux,[6]** Sébastien Santini,[1] Eleonora Scalco,[7] Sarah M. Schwenck,[6] Atsuko Tanaka,[4]§ Pierre Testor,[13] Thomas Vannier,[14,15,16] Flora Vincent,[4] Adriana Zingone,[7] Céline Dimier,[2,3,4] Marc Picheral,[9,10] Sarah Searson,[9,10]|| Stefanie Kandels-Lewis,[17,18] *Tara* Oceans Coordinators¶ Silvia G. Acinas,[19] Peer Bork,[17,20] Emmanuel Boss,[8] Colomban de Vargas,[2,3] Gabriel Gorsky,[9,10] Hiroyuki Ogata,[1]# Stéphane Pesant,[21,22] Matthew B. Sullivan,[6]** Shinichi Sunagawa,[17] Patrick Wincker,[14,15,16] Eric Karsenti,[4,18]* Chris Bowler,[4]* Fabrice Not,[2,3]*†† Pascal Hingamp,[1]*†† Daniele Iudicone[7]*††

Agulhas rings provide the principal route for ocean waters to circulate from the Indo-Pacific to the Atlantic basin. Their influence on global ocean circulation is well known, but their role in plankton transport is largely unexplored. We show that, although the coarse taxonomic structure of plankton communities is continuous across the Agulhas choke point, South Atlantic plankton diversity is altered compared with Indian Ocean source populations. Modeling and in situ sampling of a young Agulhas ring indicate that strong vertical mixing drives complex nitrogen cycling, shaping community metabolism and biogeochemical signatures as the ring and associated plankton transit westward. The peculiar local environment inside Agulhas rings may provide a selective mechanism contributing to the limited dispersal of Indian Ocean plankton populations into the Atlantic.

The Agulhas Current, which flows down the east coast of Africa, leaks from the Indo-Pacific Ocean into the Atlantic Ocean (*1*). This leakage, a choke point to heat and salt distribution across the world's oceans, has been increasing over the last decades (*2*). The influence of the Agulhas leakage on global oceanic circulation makes this area a sensitive lever in climate change scenarios (*3*). Agulhas leakage has been a gateway for planetary-scale water transport since the early Pleistocene (*4*), but diatom fossil records suggest that it is not a barrier to plankton dispersal (*5*). Most of the Agulhas leakage occurs through huge anticyclonic eddies known as Agulhas rings. These 100- to 400-km-diameter rings bud from Indian Ocean subtropical waters at the Agulhas Retroflection (*1*). Each year, up to half a dozen Agulhas rings escape the Indian Ocean, enter Cape Basin, and drift northwesterly across the South Atlantic, reaching the South American continent over the course of several years (*1*, *6*). During the transit of Agulhas rings, strong westerly "roaring forties" winds prevalent in the southern 40s and 50s latitudes cause intense internal cooling and mixing (*7*).

We studied the effect of Agulhas rings and the environmental changes they sustain on plankton dispersal. Plankton such as microalgae, which produce half of the atmospheric oxygen derived from photosynthesis each year, are at the base of open-ocean ecosystem food chains, thus playing an essential role in the functioning of the biosphere. Their dispersal is critical for marine ecosystem resilience in the face of environmental change (*8*). As part of the *Tara* Oceans expedition (*9*), we describe taxonomic and functional plankton assemblages inside Agulhas rings and across the three oceanic systems that converge at the Agulhas choke point: the western Indian Ocean subtropical gyre, the South Atlantic Ocean gyre, and the Southern Ocean below the Antarctic Circumpolar Current (Fig. 1).

Physical and biological oceanography of the sampling sites

The Indian, South Atlantic, and Southern Oceans were each represented by three sites sampled between May 2010 and January 2011 (Fig. 1 and table S1). A wide range of environmental conditions were encountered (*10*). We first sampled the two large contiguous Indian and South Atlantic subtropical gyres and the Agulhas ring structures that maintain the physical connection between them. On the western side of the Indian Ocean, station TARA_052 was characterized by tropical, oligotrophic conditions. Station TARA_064 was located within an anticyclonic eddy representing the Agulhas Current recirculation. Station TARA_065 was located at the inner edge of the Agulhas Current on the South African slope that feeds the Agulhas retroflection and Agulhas ring formation (*3*). In the South Atlantic Ocean, station TARA_070, sampled in late winter, was located in the eastern subtropical Atlantic basin. Station TARA_072 was located within the tropical circulation of the South Atlantic Ocean, and Station TARA_076 was at the northwest extreme of the South Atlantic subtropical gyre. Two stations (TARA_068 and TARA_078) from the west and east South Atlantic Ocean sampled Agulhas rings. Three stations (TARA_082, TARA_084, and TARA_085) in the Southern Ocean were selected to sample the Antarctic Circumpolar Current frontal system. Station TARA_082 sampled sub-Antarctic waters flowing northward along the Argentinian slope, waters that flow along the Antarctic Circumpolar Current (*11*) with characteristics typical

[1]Aix Marseille Université, CNRS, IGS UMR 7256, 13288 Marseille, France. [2]CNRS, UMR 7144, Station Biologique de Roscoff, Place Georges Teissier, 29680 Roscoff, France. [3]Sorbonne Universités, Université Pierre et Marie Curie UPMC, Université Paris 06, UMR 7144, Station Biologique de Roscoff, Place Georges Teissier, 29680 Roscoff, France. [4]Ecole Normale Supérieure, Institut de Biologie de l'ENS (IBENS), and Inserm U1024, and CNRS UMR 8197, F-75005 Paris, France. [5]Laboratoire de Physique des Océans (LPO) UMR 6523 CNRS-Ifremer-IRD-UBO, Plouzané, France. [6]Department of Ecology and Evolutionary Biology, University of Arizona, Tucson, AZ 85721, USA. [7]Stazione Zoologica Anton Dohrn, Villa Comunale, 80121 Naples, Italy. [8]School of Marine Sciences, University of Maine, Orono, ME, USA. [9]Sorbonne Universités, UPMC Université Paris 06, Observatoire Océanologique, F-06230 Villefranche-sur-Mer, France. [10]INSU-CNRS, UMR 7093, LOV, Observatoire Océanologique, F-06230 Villefranche-sur-Mer, France. [11]Department of Earth, Atmospheric and Planetary Sciences, Massachusetts Institute of Technology, Cambridge, MA, USA. [12]Université de Toulon, Laboratoire PROTEE-EBMA E.A. 3819, BP 20132, 83957 La Garde Cedex, France. [13]CNRS, UMR 7159, Laboratoire d'Océanographie et du Climat LOCEAN, 4 Place Jussieu, 75005 Paris, France. [14]Commissariat à l'Energie Atomique et aux Energies Alternatives (CEA), Institut de Génomique, Genoscope, 2 Rue Gaston Crémieux, 91057 Evry, France. [15]CNRS, UMR 8030, CP5706, Evry, France. [16]Université d'Evry, UMR 8030, CP5706, Evry, France. [17]Structural and Computational Biology, European Molecular Biology Laboratory, Meyerhofstrasse 1, 69117 Heidelberg, Germany. [18]Directors' Research, European Molecular Biology Laboratory, Meyerhofstrasse 1, 69117 Heidelberg, Germany. [19]Department of Marine Biology and Oceanography, Institute of Marine Sciences (ICM), CSIC, Passeig Marítim de la Barceloneta, 37-49, Barcelona E08003, Spain. [20]Max-Delbrück-Centre for Molecular Medicine, 13092 Berlin, Germany. [21]PANGAEA, Data Publisher for Earth and Environmental Science, University of Bremen, Bremen, Germany. [22]MARUM, Center for Marine Environmental Sciences, University of Bremen, Bremen, Germany. [23]Department of Geosciences, Laboratoire de Météorologie Dynamique (LMD) UMR 8539, Ecole Normale Supérieure, 24 Rue Lhomond, 75231 Paris Cedex 05, France. ***Corresponding author. E-mail: villar@igs.cnrs-mrs.fr (E.V.); not@sb-roscoff.fr (F.N.); hingamp@igs.cnrs-mrs.fr (P.H.); iudicone@szn.it (D.I.); karsenti@embl.de (E.K.), cbowler@biologie.ens.fr (C.B.)** †These authors contributed equally to this work. ‡Present address: CNRS FR3631, Institut de Biologie Paris-Seine, F-75005 Paris, France; Sorbonne Universités, UPMC Université Paris 06, Institut de Biologie Paris-Seine (IBPS), F-75005 Paris, France. §Present address: Muroran Marine Station, Field Science Center for Northern Biosphere, Hokkaido University, Japan. ||Present address: CMORE, University Hawaii, Honolulu, USA. ¶*Tara* Oceans coordinators are listed at the end of this paper. #Present address: Institute for Chemical Research, Kyoto University, Gokasho, Uji, Kyoto, 611-0011, Japan. **Present address: Department of Microbiology, Ohio State University, Columbus, OH 43210, USA. ††These authors contributed equally to this work.

of summer sub-Antarctic surface waters and are stratified by seasonal heating. Station TARA_084 was located on the southern part of the Antarctic Circumpolar Current, in the Drake Passage between the Polar Front and the South Antarctic Circumpolar Current front (*11*). Station TARA_085 was located on the southern edge of the South Antarctic Circumpolar Current front with waters typical of polar regions.

We compared overall plankton community structures between the three oceans using imaging and genetic surveys of samples from the epipelagic zone of each station (*12*). Prokaryote, phyto-, and zooplankton assemblages were similar across Indian and South Atlantic Ocean samples but different from Southern Ocean samples (Fig. 2A). In the Indian and South Atlantic Oceans, zooplankton communities were dominated by Calanoida, Cyclopoida (Oithonidae), and Poecilostomatoida copepods (*12*); phytoplankton communities were mainly composed of chlorophytes, pelagophytes, and haptophytes (*12*). In contrast, Southern Ocean zooplankton communities were distinguished by an abundance of *Limacina* spp. gastropods and Poecilostomatoida copepods. Southern Ocean phytoplankton were primarily diatoms and haptophytes. The divergence was even more conspicuous with respect to prokaryotes, in that picocyanobacteria, dominant in the Indian and South Atlantic Oceans, were absent in the Southern Ocean. The Southern Ocean had a high proportion of Flavobacteria and Rhodobacterales (*12*). Virus concentrations in the <0.2-μm size fractions were significantly lower in the southernmost Southern Ocean station (*13*). Viral particles were significantly smaller in two of the three Southern Ocean sampling sites, and two Southern Ocean viromes had significantly lower richness compared with the South Atlantic and Indian Oceans (*13*). Although nucleocytoplasmic large DNA viruses were similarly distributed in the South Atlantic and Indian Oceans (*12*), two Southern Ocean sites contained coccolithoviruses also found in the TARA_068 Agulhas ring but not in the other Indian and South Atlantic stations.

Biological connection across the Agulhas choke point

Genetic material as represented by ribosomal RNA gene (rDNA) sequences showed exchange patterns across the oceans (shared barcode richness) (*14*). Despite a smaller interface between the Indian and South Atlantic Oceans than either have with the Southern Ocean, more than three times as much genetic material was in common between the Indian and South Atlantic Oceans than either had with the Southern Ocean (Fig. 2B) (*15*). Indeed, the Indian–South Atlantic interocean shared barcodes richness (32 ± 5%) was not significantly different from typical intraocean values (37 ± 7%, Tukey post hoc, 0.95 confidence). Shared barcode richness involving the Southern Ocean was significantly lower (9 ± 3%) (Fig. 2C). We found that the proportion of whole shotgun metagenomic reads shared between samples, both intraoceanic and Indian–South Atlantic interocean similarities, were in the 18 to 30% range, whereas interocean similarities with Southern Ocean samples were only 5 to 6% (*16*). The statistically indistinguishable Indo-Atlantic intra- and interocean genetic similarities revealed a high Indo-Atlantic biological connection despite the physical basin discontinuity.

Nonetheless, differences on either side of the Agulhas choke point were evident. We found that prokaryote barcode richness was greater in the South Atlantic than in the Indian Ocean (Fig. 3A) (0.2- to 3-μm size fraction). The opposite trend characterized eukaryotes larger than 20 μm in size. We cannot rule out the possibility that the higher prokaryote diversity observed in the South Atlantic Ocean might be due to a protocol artifact resulting from a difference in prefiltration pore size from 1.6 μm (Indian Ocean) to 3 μm (South Atlantic and Southern Oceans). As also evident from the panoceanic *Tara* Oceans data set (*17*), smaller size fractions showed greater eukaryote diversity across the Agulhas system. In all size fractions that we analyzed, samples from the Southern Ocean were less diverse than samples from the South Atlantic Ocean and Indian Ocean (Fig. 3A).

When rDNA barcodes were clustered by sequence similarity and considered at operational taxonomic unit (OTU) level (*14*), more than half (57%) of the OTUs contained higher sub-OTU barcode richness in the Indian Ocean than in the South Atlantic Ocean, whereas less than a third (32%) of OTUs were richer in the South Atlantic Ocean, leaving only 11% as strictly cosmopolitan (Fig. 3B). Taken together, these 1307 OTUs represented 98% of the barcode abundance, indicating that the observed higher barcode richness within OTUs in the Indian Ocean was not conferred by the rare biosphere. Certain taxa displayed unusual sub-OTU richness profiles across the choke point. Consistent with their relatively large size, Opisthokonta (mostly copepods), Rhizaria (such as radiolarians), and Stramenopiles (in particular diatoms) had much higher sub-OTU barcode richness in the Indian Ocean, whereas only small-sized Hacrobia (mostly haptophytes) showed modest increased sub-OTU barcode richness in the South Atlantic Ocean. The plankton filtering that we observed in fractions above 20 μm through the Agulhas choke point might explain the reduction of marine nekton diversity from the Indian Ocean to the South Atlantic Ocean (*18*) by propagating up the food web (*19*).

In situ sampling of two Agulhas rings

To understand whether the environment of Agulhas rings, the main transporters of water across the choke point, might act as a biological filter between the Indian Ocean and the South Atlantic Ocean, we analyzed data collected in both a young and an old Agulhas ring. The young ring sampled at station TARA_068 was located in the Cape Basin, west of South Africa, where rings are often observed after their formation at the Agulhas Retroflection (*7*, *20*). It was a large Agulhas ring that detached from the retroflection about 9 to 10 months before sampling. This ring first moved northward and then westward in the Cape Basin while interacting with other structures (red track in Fig. 1) (*21*). Ocean color data collected by satellite showed that surface chlorophyll concentrations were higher in the Cape Basin than at the retroflection, suggesting that vigorous vertical

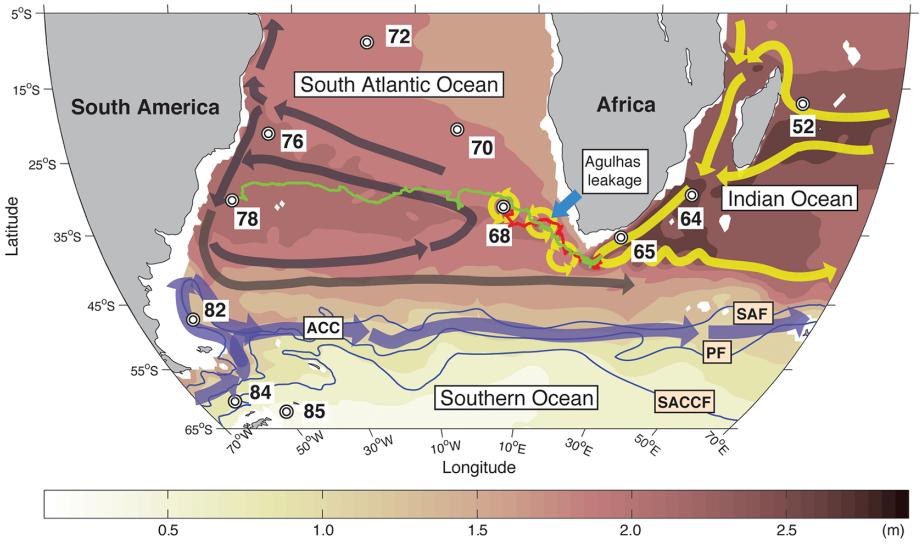

Fig. 1. The oceanic circulation around the Agulhas choke point and location of *Tara* Oceans stations. The map shows the location of sampling stations, together with trajectories of the young and old Agulhas rings (TARA_068 and TARA_078, red and green tracks, respectively). The stations here considered as representative of the main basins are (i) TARA_052, TARA_064, and TARA_065 for Indian Ocean; (ii) TARA_070, TARA_072, and TARA_076 for the South Atlantic Ocean, and (iii) TARA_082, TARA_084, and TARA_085 for the Southern Ocean. The mean ocean circulation is schematized by arrows (currents) and background colors [surface climatological dynamic height (0/2000 dbar from CARS2009; www.cmar.csiro.au/cars)] (*70*). Agulhas rings are depicted as circles. The Antarctic Circumpolar Current front positions are from (*13*).

mixing might have occurred in the Cape Basin (*22*). At the time of sampling, the anticyclonic Agulhas ring was 130 to 150 km in diameter, was about 30 cm higher than average sea surface height, and was flanked by a 130- to 150-km cyclonic eddy to the north and a larger (>200 km) one to the east (Fig. 4A) (*23*). Thermosalinograph data showed that filaments of colder, fresher water surrounded the young ring core (Fig. 4A) (*23*). To position the biological sampling station close to the ring core, a series of conductivity-temperature-depth (CTD) casts was performed (*23*, *24*). The young Agulhas ring had a surface temperature and salinity of 16.8°C and 35.7 practical salinity units (PSU), respectively, and the isopycnal sloping could be traced down to CTD maximal depth (900 to 1000 m). The core of the ring water was 5°C cooler than Indian Ocean subtropical source waters at similar latitudes (TARA_065) (table S1), typical for the subtropical waters south of Africa (17.8°C, 35.56 PSU, respectively) (*25*). The mixed layer of the young ring was deep (>250 m) compared with seasonal cycles of the mixed layer depths in the region (50 to 100 m) (Fig. 4C), typical of Agulhas rings (*26*). At larger scales (Fig. 4B) (*24*), steep spatial gradients were observed, with fresher and colder water in the Cape Basin than in the Agulhas Current because of both lateral mixing with waters from the south and surface fluxes. This confirms that the low temperature of the young Agulhas ring is a general feature of this Indian to South Atlantic Ocean transitional basin. Air-sea exchanges of heat and momentum promoted convection in the ring core, which was not compensated by lateral mixing and advection. The core of the Agulhas ring thus behaved as a subpolar environment traveling across a subtropical region.

At station TARA_078, we sampled a second structure whose origins were in the Agulhas Retroflection, likely a 3-year-old Agulhas ring. This old ring, having crossed the South Atlantic Ocean, was being absorbed by the western boundary current of the South Atlantic subtropical gyre. The structure sampled at station TARA_078 was characterized by a warm salty core (*27*). As for the young Agulhas ring sampled, the old ring also had a 100-m-deeper pycnocline than surrounding waters, typical of large anticyclonic structures.

The plankton assemblage of both Agulhas rings most closely resembled the assemblages found in Indian and South Atlantic samples (Fig. 2A). At higher resolution, barcodes (Fig. 2, B and C) and metagenomic reads (*16*) shared between the Agulhas rings and the Indian or South Atlantic samples showed that the young ring was genetically distinct from both Indian and South Atlantic samples,

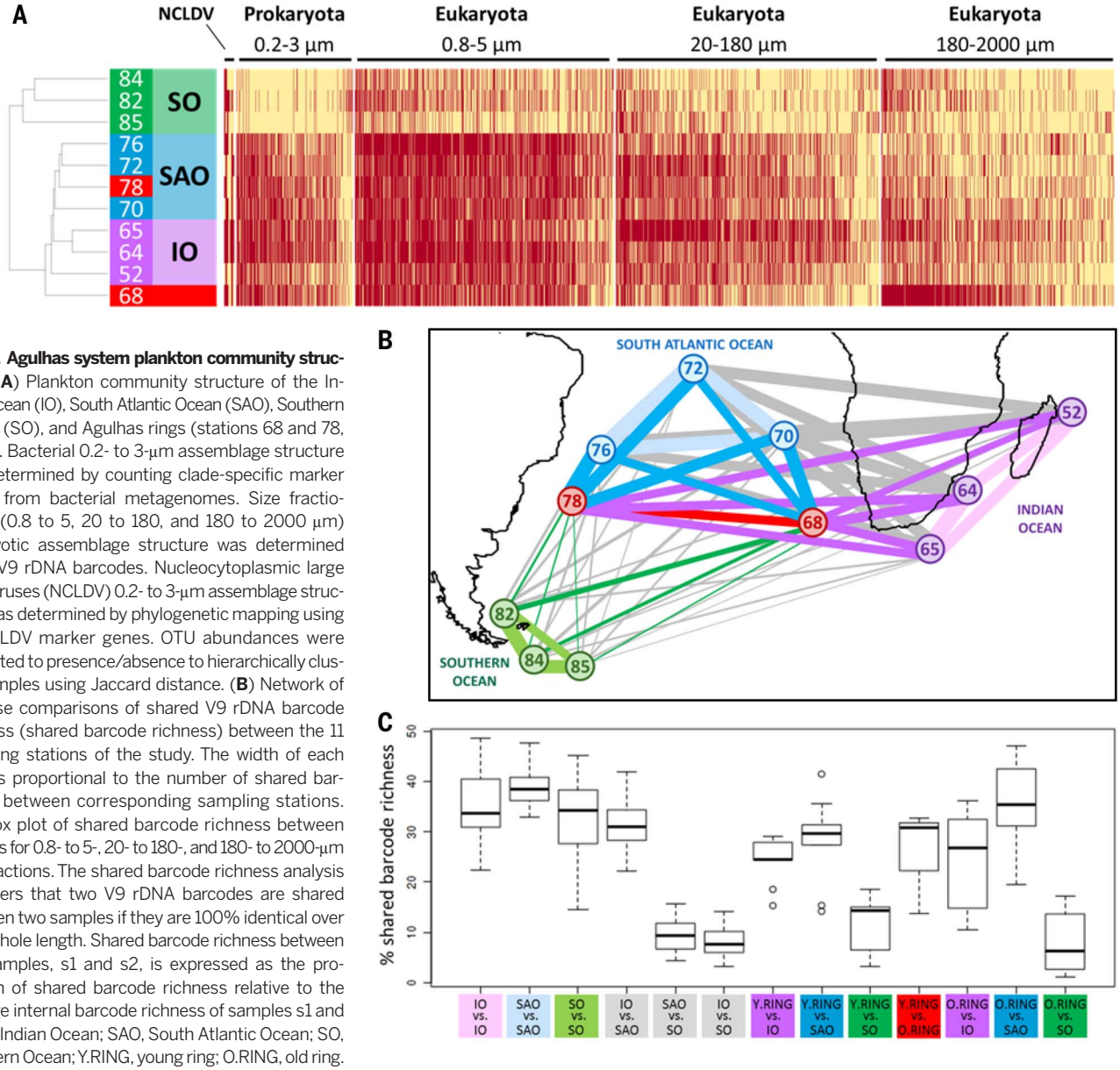

Fig. 2. Agulhas system plankton community structure. (**A**) Plankton community structure of the Indian Ocean (IO), South Atlantic Ocean (SAO), Southern Ocean (SO), and Agulhas rings (stations 68 and 78, in red). Bacterial 0.2- to 3-µm assemblage structure was determined by counting clade-specific marker genes from bacterial metagenomes. Size fractionated (0.8 to 5, 20 to 180, and 180 to 2000 µm) eukaryotic assemblage structure was determined using V9 rDNA barcodes. Nucleocytoplasmic large DNA viruses (NCLDV) 0.2- to 3-µm assemblage structure was determined by phylogenetic mapping using 16 NCLDV marker genes. OTU abundances were converted to presence/absence to hierarchically cluster samples using Jaccard distance. (**B**) Network of pairwise comparisons of shared V9 rDNA barcode richness (shared barcode richness) between the 11 sampling stations of the study. The width of each edge is proportional to the number of shared barcodes between corresponding sampling stations. (**C**) Box plot of shared barcode richness between stations for 0.8- to 5-, 20- to 180-, and 180- to 2000-µm size fractions. The shared barcode richness analysis considers that two V9 rDNA barcodes are shared between two samples if they are 100% identical over their whole length. Shared barcode richness between two samples, s1 and s2, is expressed as the proportion of shared barcode richness relative to the average internal barcode richness of samples s1 and s2. IO, Indian Ocean; SAO, South Atlantic Ocean; SO, Southern Ocean; Y.RING, young ring; O.RING, old ring.

whereas the old ring was similar to its surrounding South Atlantic samples (Tukey post hoc, 0.95 confidence). Light microscopy analyses revealed some plankton groups specific to the young Agulhas ring, such as *Pseudo-nitzschia* spp., which represented 20% of the phytoplankton counts but less than 10% in all other stations (*12*). Other potentially circumstantial plankton characteristic of the young Agulhas ring included the tintinnid *Dictyocysta pacifica* (*12*), the diatom *Corethron pennatum* (*12*), and the dinoflagellate *Tripos limulus* (*12*). A tiny (less than 15 μm long) pennate diatom from the genus *Nanoneis,* which we saw only in the young Agulhas ring and Indian Ocean stations around the African coasts (*28*), was an example of the Indo-Atlantic plankton diversity filtering observed at rDNA barcode level and corroborated by microscopy. OTU clustered barcodes revealed a variety of young Agulhas ring sub-OTU richness patterns compared with source and destination oceans (Fig. 5A). Among Copepoda, *Gaetanus variabilis* and *Corycaeus speciosus* were the more cosmopolitan species (Fig. 5B), whereas *Bradya* species found in the young ring were mainly similar to those from the Indian Ocean. *Acartia negligens* and *Neocalanus robustior* displayed high levels of barcode richness specific to each side of the Agulhas choke point. Bacillariophyceae were heavily filtered from Indian to South Atlantic Oceans (Fig. 5C), and most OTUs (17 out of 20) were absent in the young ring, suggesting that diversity filtering could take place earlier in the ring's 9-month history. Consistent with the observed particularities of the plankton in the young ring, continuous underway optical measurements showed that the ring core photosynthetic community differed from surrounding waters (*29*–*31*). Intermediate size cells, and relatively low content of photoprotective pigments, reflected low growth irradiance and suggested a transitional physiological state. Thus, the plankton community in the young Agulhas ring had diverged from plankton communities typical of its original Indian waters but, even 9 months after formation, had not converged with its surrounding South Atlantic waters.

Deep mixing in Agulhas rings promotes plankton bloom

The upper water column of the young ring showed a high nitrite concentration (>0.5 mmol m^{-3}) (Fig. 4D) (*32*). This observation, along with its particularly deep mixed layer (>250 m), suggested that as Agulhas rings proceed westward in the Cape Basin, vigorous deep mixing of their weakly stratified waters may have entrained nitrate and stimulated phytoplankton blooms. Typically, fresh organic material would then either be exported as sinking particles or locally recycled, sustaining heterotrophic production of ammonium that would, in turn, be consumed by photoautotrophs in the euphotic layer but nitrified below. The resulting nitrite, eventually oxidized to nitrate, might remain evident at subsurface as observed in the nitrite anomaly of the young ring detected here. This hypothesis was supported by numerical simulations of the Massachusetts Institute of Technology General Circulation Model (*33*), which resolved Agulhas rings, their phytoplankton populations, and associated nutrient cycling (Fig. 6A). We tracked 12 Agulhas rings in the ocean model and characterized their near-surface biogeochemical cycles (Fig. 6B) (*34*). As the rings moved westward, storms enhanced surface heat loss, stimulating convection and the entrainment of nitrate. In the model simulations, proliferation of phytoplankton generated subsurface nitrite, which persisted because phytoplankton were light-limited at depth and because nitrification was suppressed by light at the surface (*35*). The associated blooms were dominated by large opportunistic phytoplankton and nitrate-metabolizing *Synechococcus* spp. analogs, whereas populations of *Prochlorococcus* spp. analogs dominated the quiescent periods (*34*). Each of the 12 simulated Agulhas rings exhibited this pattern in response to surface forcing by weather systems, and all rings maintained a persistent

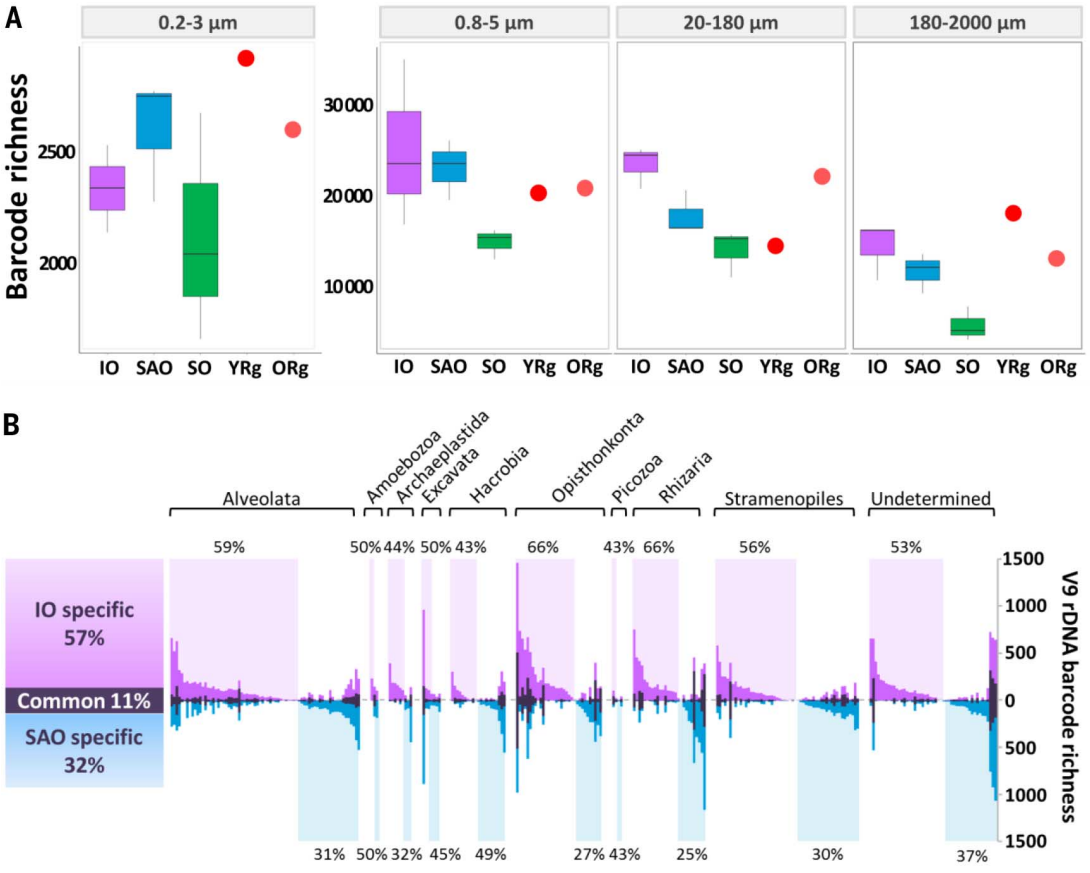

Fig. 3. Diversity of plankton populations specific to Indian and Atlantic Oceans. (**A**) Box plot of 16S (0.2 to 3 μm) and V9 rDNA barcodes richness (0.8- to 5-, 20- to 180-, and 180- to 2000-μm size fractions). Each box represents three sampling stations combined into Indian, South Atlantic, and Southern Ocean. Single Agulhas ring stations are represented as red (young ring) and orange (old ring) crosses. (**B**) Plankton sub-OTU richness filtering across the Agulhas choke point. Each vertical bar represents a single eukaryotic plankton OTU, each of which contains >10 distinct V9 rDNA barcodes (*14*). For each OTU are represented the number of distinct barcodes (sub-OTU richness) found exclusively in the South Atlantic Ocean (blue), exclusively in the Indian Ocean (pink), and in both South Atlantic Ocean and Indian Ocean (gray). OTUs are grouped by taxonomic annotation (indicated above the bar plot). For each taxonomic group, the percentage of OTUs with higher sub-OTU richness in the Indian Ocean (shaded in pink) or in the South Atlantic Ocean (shaded in blue) is indicated, respectively, at the top and bottom of the bar plot. A total of 1307 OTUs are presented, representing 98% of total V9 rDNA barcode abundance.

subsurface nitrite maximum in the region, as observed in TARA_068 and in other biogeochemical surveys (*36*).

The nitrite peak observed at TARA_068 in the young Agulhas ring was associated with a differential representation of nitrogen metabolism genes between the ring and the surrounding South Atlantic and Indian Oceans metagenomes derived from 0.2- to 3-μm size fractions (Fig. 7) (*37*). Agulhas ring overrepresented KEGG (Kyoto Encyclopedia of Genes and Genomes) orthologs (KOs) were involved in both nitrification and denitrification, likely representing the overlap between plankton assemblages involved in the conversion of nitrate to nitrite on the one hand and in denitrification of the accumulating nitrite on the other. Distinct KOs involved in successive denitrification steps were found to be encoded by similar plankton taxa. For instance, KO10945 and KO10946 (involved in ammonium nitrification) and KO00368 (subsequently involved in nitrite to nitrous oxide denitrification) appeared mostly encoded by Nitrosopumilaceae archaea. KO00264 and KO01674 (involved in ammonium assimilation) were mostly assigned to eukaryotic Mamiellales, whereas the opposite KO00367 and KO00366 (involved in dissimilatory nitrite reduction to ammonium), followed by KO01725 (involved in ammonium assimilation), were encoded by picocyanobacteria. In the specific case of the picocyanobacteria, metagenomic reads corresponding to *nirA* genes showed that the observed young Agulhas ring KO00366 (dissimilatory nitrite reduction) enrichment was mainly due to the overrepresentation of genes from *Prochlorococcus* (Fig. 8B). This enrichment was found to be associated with a concomitant shift in population structure from *Prochlorococcus* high-light II ecotypes (HLII, mostly lacking *nirA* genes) to codominance of high-light I (HLI) and low-light I (LLI) ecotypes. Indeed, among the several *Prochlorococcus* and *Synechococcus* ecotypes identified based on their genetic diversity and physiology (*38*, *39*), neutral marker (*petB*) (Fig. 8A) recruitments showed that dominant clades in the Indian Ocean upper mixed layer were *Prochlorococcus* HLII and *Synechococcus* clade II, as expected given the known (sub)tropical preference of these groups (*40*). Both clades nearly completely disappeared (less than 5%) in the mixed cold waters of the young ring and only began to increase again when the surface water warmed up along the South Atlantic Ocean transect. Conversely, young ring water was characterized by a large proportion of *Prochlorococcus* HLI and LLI and *Synechococcus* clade IV, two clades typical of temperate waters. Besides temperature, the *Prochlorococcus* community shift from HLII to HLI + LLI observed in the young ring was likely also driven by the nitrite anomaly. Indeed, whereas most *Synechococcus* strains isolated so far are able to

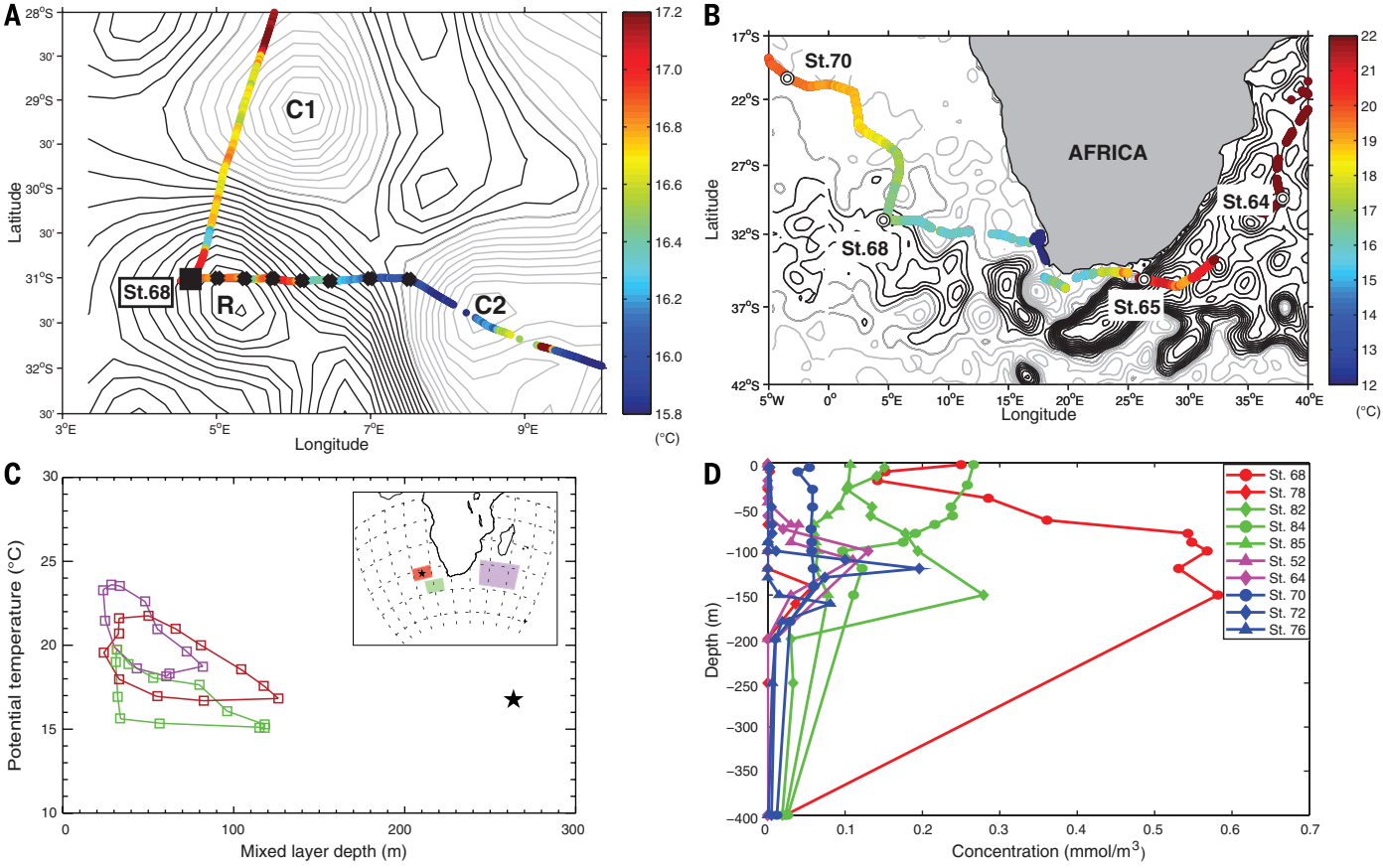

Fig. 4. Properties of the young Agulhas ring (TARA_068). (**A**) Daily sea surface height around young Agulhas ring station TARA_068 [absolute dynamic topography (ADT) from www.aviso.altimetry.fr]. R, C1, and C2, respectively, denote the centers of the Agulhas ring and two cyclonic eddies. The contour interval is 0.02 dyn/m. The ADT values are for 13 September 2010. Light gray isolines, ADT < 0.46 dyn/m. The crosses indicate the CTD stations, and the square symbol indicates the position of the biological station TARA_068. The biological station coincides with the westernmost CTD station. ADT is affected by interpolation errors, which is why CTD casts were performed at sea so as to have a fine-scale description of the feature before defining the position of the biological station (*23*). Superimposed are the continuous underway temperatures (°C) from the on-board thermosalinograph. (**B**) Same as (A) but at the regional scale. Round symbols correspond to biological sampling stations. The contour interval is 0.1 dyn/m. (**C**) Seasonal distribution of the median values of the mixed layer depths and temperatures at 10 m (from ARGO) provided by the IFREMER/LOS Mixed Layer Depth Climatology L2 database (www.ifremer.fr/cerweb/deboyer/mld) updated to 27 July 2011. The mixed layer is defined using a temperature criterion. The star symbol represents the young ring station TARA_068. (Inset) Geographic position of the areas used to select the mixed layer and temperature data. The mixed layer depth measured at TARA_068 is outside the 90th percentile of the distribution of mixed layer depths for the same month for both the subtropical (red and magenta) regions. The temperature matches the median for the same month and region of sampling. (**D**) Nitrite (NO_2) concentrations from CTD casts at different sampling sites (expressed in mmol/m^3).

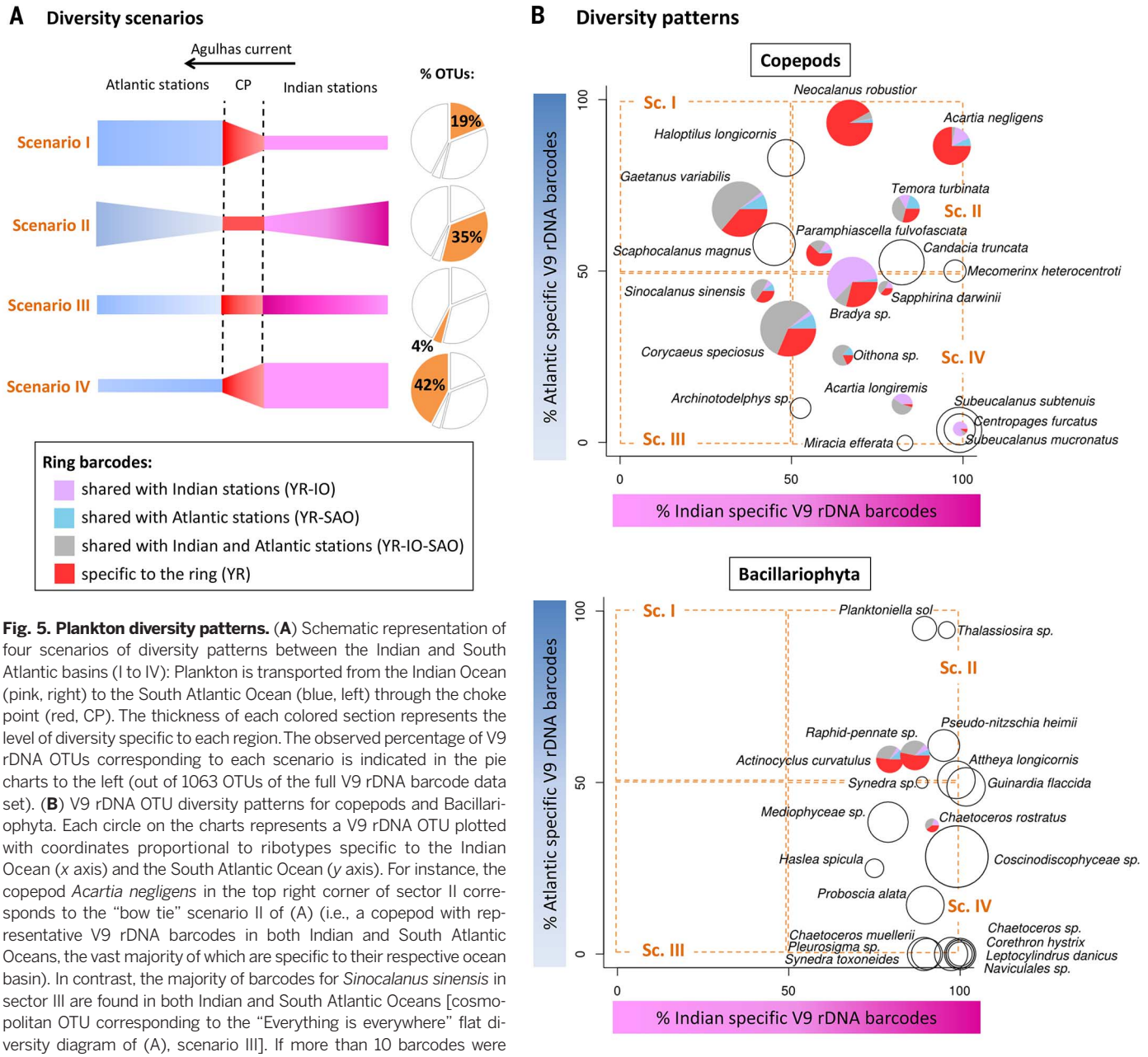

Fig. 5. Plankton diversity patterns. (**A**) Schematic representation of four scenarios of diversity patterns between the Indian and South Atlantic basins (I to IV): Plankton is transported from the Indian Ocean (pink, right) to the South Atlantic Ocean (blue, left) through the choke point (red, CP). The thickness of each colored section represents the level of diversity specific to each region. The observed percentage of V9 rDNA OTUs corresponding to each scenario is indicated in the pie charts to the left (out of 1063 OTUs of the full V9 rDNA barcode data set). (**B**) V9 rDNA OTU diversity patterns for copepods and Bacillariophyta. Each circle on the charts represents a V9 rDNA OTU plotted with coordinates proportional to ribotypes specific to the Indian Ocean (*x* axis) and the South Atlantic Ocean (*y* axis). For instance, the copepod *Acartia negligens* in the top right corner of sector II corresponds to the "bow tie" scenario II of (A) (i.e., a copepod with representative V9 rDNA barcodes in both Indian and South Atlantic Oceans, the vast majority of which are specific to their respective ocean basin). In contrast, the majority of barcodes for *Sinocalanus sinensis* in sector III are found in both Indian and South Atlantic Oceans [cosmopolitan OTU corresponding to the "Everything is everywhere" flat diversity diagram of (A), scenario III]. If more than 10 barcodes were found in the young Agulhas ring (TARA_068), their distribution is indicated in a pie chart (colors are coded in the legend inset); otherwise, the OTU is represented by an empty circle. Circle sizes are proportional to the number of considered barcodes for each OTU. The Bacillariophyta OTU defined as *Raphid pennate* sp. likely corresponds to the *Pseudo-nitzschia* cells observed by light microscopy.

use nitrate, nitrite, and ammonium, only the *Prochlorococcus* LLI and IV and some populations of HL clades, having acquired the *nirA* gene by lateral gene transfer, are able to assimilate nitrite. In the young ring, overrepresentation of cyanobacterial orthologs involved in nitrite reduction could thus have resulted from environmental pressure selecting LLI (87% of the *nirA* recruitments) and HL populations (13%) that possessed this ability. Because the capacity to assimilate nitrite in this latter ecotype reflects the availability of this nutrient in the environment (*41*), these in situ observations of picocyanobacteria indicated that the nitrogen cycle disturbance occurring in the young ring exerts community-wide selective pressure on Agulhas ring plankton.

Discussion

We found that whether or not the Agulhas choke point is considered a barrier to plankton dispersal depends on the taxonomic resolution at which the analysis is performed. At coarse taxonomic resolution, our observations of Indo-Atlantic continuous plankton structure—from viruses to fish larvae—suggested unlimited dispersal, consistent with previous reports (*5*, *42*). However, at finer resolution, our genetic data revealed that the Agulhas choke point strongly affects patterns of plankton genetic diversity. As anticipated in (*5*), the diversity filtering by Agulhas rings likely escaped detection using fossil records because of the limited taxonomic resolution afforded by fossil diatom morphology (*42*). The community-wide evidence presented here confirms observations on individual living species (*43*, *44*), suggesting that dispersal filters mitigate the panmictic ocean hypothesis for plankton above 20 μm.

The lower diversity we observed in the South Atlantic Ocean for micro- and mesoplankton (>20 μm) may be due to local abiotic/biotic pressure or to limitations in dispersal (*33*, *45*). Biogeography emerging from a model with only neutral drift (*46*) predicts

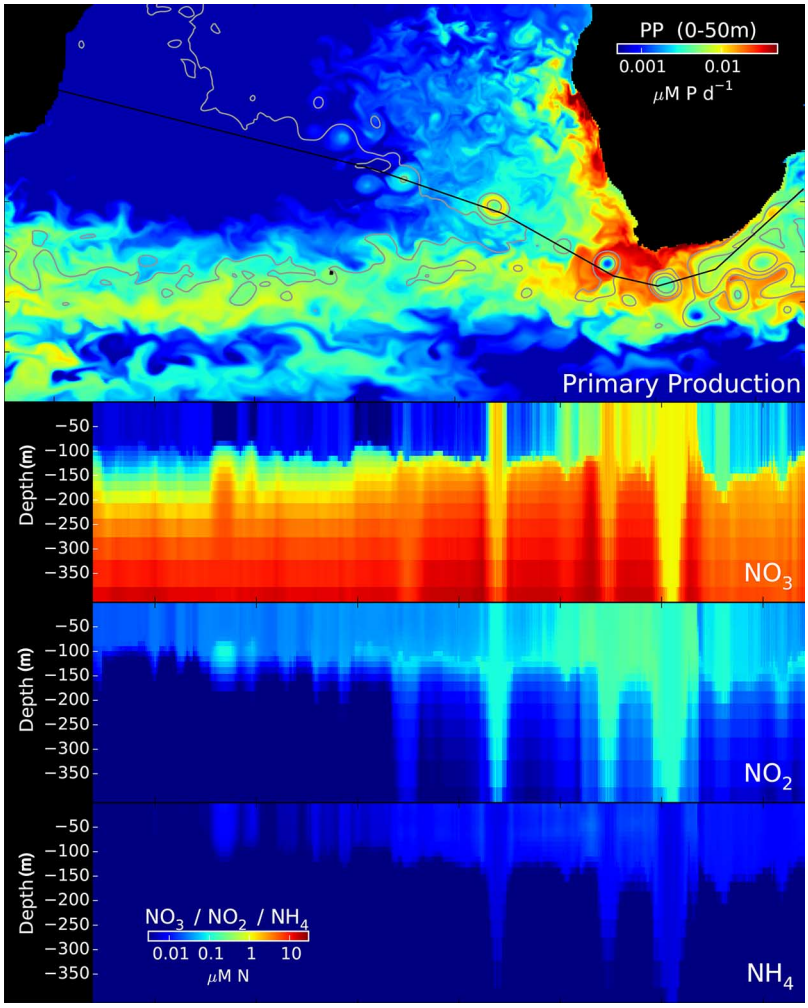

Fig. 6. Modeled nitrogen stocks along Agulhas ring track. (**Top**) Simulated primary production (PP) in the Agulhas system using the MIT-GCM model. The solid black line shows the average northwesterly path of 12 distinct virtual Agulhas rings tracked over the course of the simulation. Color scale for PP is given in the top right inset, with warmer colors indicating higher PP. (**Bottom**) Modeled profiles of NO_3, NO_2, and NH_4 along the Agulhas ring average track (*x* axis) presented in (A). The *y* axis is the depth (in meters) in the water column. The color scale is given in the bottom left inset, with warmer colors indicating higher concentrations of nitrogen compounds.

basin-to-basin genetic differences that are qualitatively consistent with our data. However, the increased proportion of *Prochlorococcus* HL populations carrying the *nirA* gene in the young Agulhas ring indicates that selection is at work in Agulhas rings. Based on our analysis of two Agulhas rings, we propose that environmental disturbances in Agulhas rings reshape their plankton diversity as they travel from the Indian Ocean to the South Atlantic Ocean. Such selective pressure may contribute to the South Atlantic Ocean plankton diversity shift relative to its upstream Indo-Pacific basin. Thus, environmental selection applied at a choke point in ocean circulation may constitute a barrier to dispersal (*47*, *48*). Furthermore, we show that taxonomic groups were not equally affected by the ring transport, both within and between phyla, with a noticeable effect of organism size. The differential effects due to organism size highlight the difficulty in generalizing ecological and evolutionary rules from limited sampling of species or functional types.

Considering the sensitivity of Agulhas leakage to climate change (*1*, *49*), better understanding of the plankton dynamics in Agulhas rings will be required if we are to understand and predict ecosystem resilience at the planetary scale. Considering the breadth of changes already observed in the 9-month-old Agulhas ring, it would be interesting to acquire samples from specific Agulhas rings tracked from early formation to dissipation. Finally, our data suggest that the abundance of Indian Ocean species in South Atlantic Ocean sedimentary records, used as proxies of Agulhas leakage intensity (*4*), may actually also depend on the physical and biological characteristics of the Agulhas rings.

Materials and methods

Sampling

The *Tara* Oceans sampling protocols schematized in Karsenti *et al.* (*9*) are described in Pesant *et al.* (*50*); specific methods for 0.8- to 5-, 20- to 180-, and 180- to 2000-μm size fractions in de Vargas *et al.* (*17*); for 0.2- to 3-μm size fractions in Sunagawa *et al.* (*51*); and for <0.2-μm size fraction in Brum *et al.* (*52*). Due to their fragility, 1.6-μm glass fiber filters initially used for prokaryote sampling were replaced by more resistant 3-μm polycarbonate filters from station TARA_066 onward. In the present text, both 0.2- to 1.6-μm and 0.2- to 3-μm prokaryote size fractions are simply referred to as 0.2 to 3 μm.

Data acquisition

A range of analytical methods covering different levels of taxonomic resolution (pigments, flow cytometry, optical microscopy, marker gene barcodes, and metagenomics) were used to describe the planktonic composition at each sampled station. Viruses from the <0.2 μm size fraction were studied by epifluorescence microscopy, by quantitative transmission electron microscopy, and by sequencing DNA as described in Brum *et al.* (*52*). Flow cytometry was used to discriminate high-DNA-content bacteria (HNA), low-DNA-content bacteria (LNA), *Prochlorococcus* and *Synechococcus* picocyanobacteria, and two different groups (based on their size) of photosynthetic picoeukaryotes, as described previously (*53*). Pigment concentrations measured by high-performance liquid chromatography (HPLC) were used to estimate the dominant classes of phytoplankton using the CHEMTAX procedure (*54*). Tintinnids, diatoms, and dinoflagellates were identified and counted by light microscopy from the 20- to 180-μm lugol or formaldehyde fixed-size fraction. Zooplankton enumeration was performed on formol fixed samples using the ZOOSCAN semi-automated classification of digital images (*55*). Sequencing, clustering, and annotation of 18*S*-V9 rDNA barcodes are described in de Vargas *et al.* (*17*). Metagenome sequencing, assembly, and annotation are described in Sunagawa *et al.* (*51*). NCLDV taxonomic assignations in the 0.2- to 3-μm samples were carried out using 18 lineage-specific markers as described in Hingamp *et al.* (*56*). Virome sequencing and annotation are described in Brum *et al.* (*52*). Samples and their associated contextual data are described at PANGAEA (*57*–*59*).

Data analysis

Origin of sampled Agulhas rings

Using visual and automated approaches, the origins of the TARA_068 and TARA_078 stations were traced back from the daily altimetric data (Fig. 1) (*21*). The automated approach used either the Lagrangian tracing of numerical particles initialized in the center of a given structure and transported by the geostrophic velocity field calculated from sea surface height gradients, or the connection in space and time of adjacent extreme values in sea level anomaly maps.

V9 rDNA barcodes

To normalize for differences in sequencing effort, V9 rDNA barcode libraries were resampled 50 times for the number of reads corresponding to the smallest library in each size fraction: 0.8 to 5 μm, 776,358 reads; 20 to 180 μm, 1,170,592 reads; and 180 to 2000 μm, 767,940 reads. V9 rDNA barcode counts were then converted to the average number

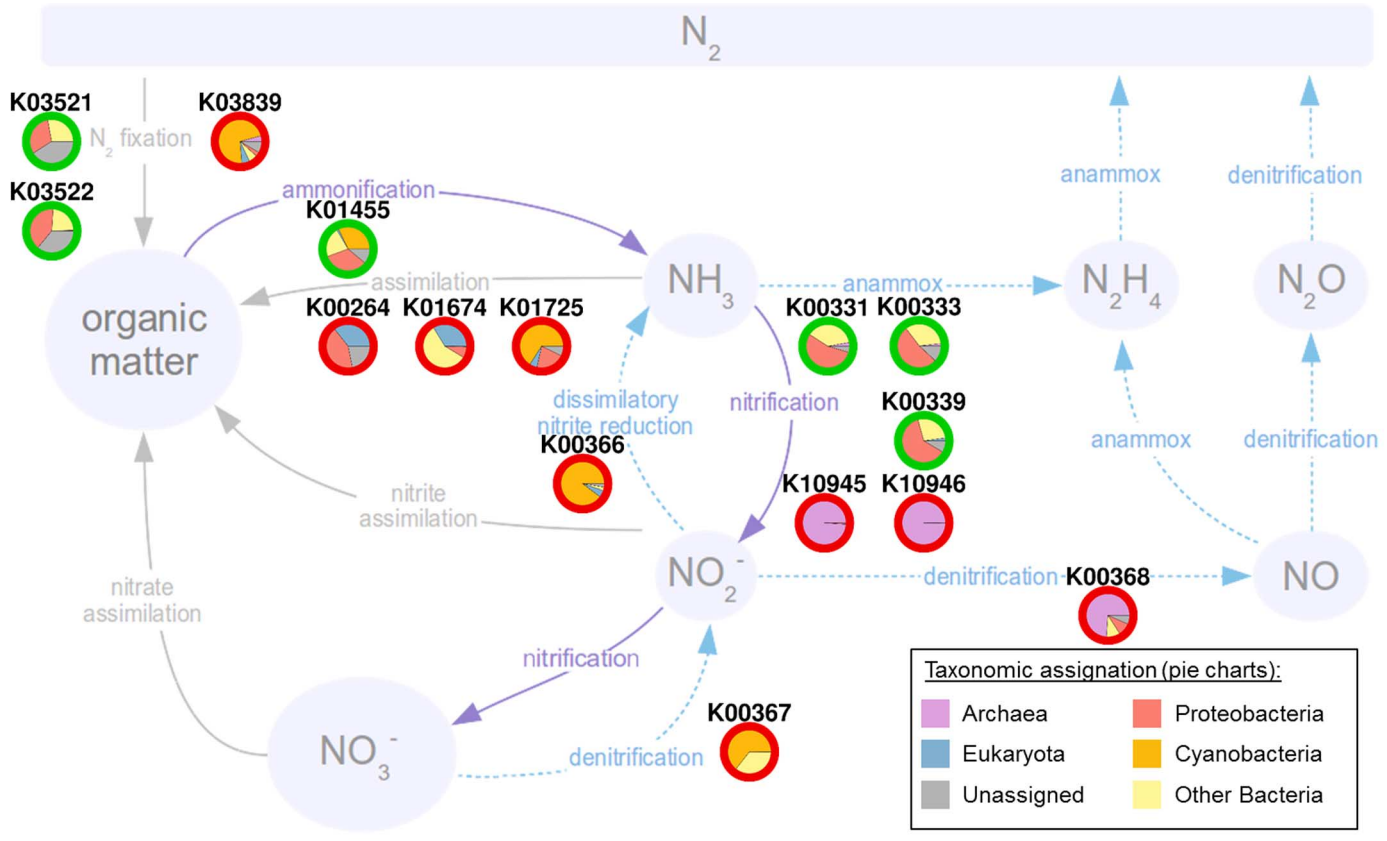

Fig. 7. Nitrite anomaly in the young Agulhas ring is accompanied by shifts in nitrogen pathway–related genes. Metagenomic over- and underrepresented nitrogen pathway genes in young Agulhas ring. Over- (red circles) and under- (green circles) represented metagenome functional annotations (KEGG Orthologs, KO#) involved in the nitrogen pathway in the young ring compared to Indian and South Atlantic Oceans reference stations, at surface and deep chlorophyll maximum depth. Pie charts inside circles represent the taxonomic distribution for each ortholog.

of times seen in the 50 resampling events, and barcodes with less than 10 reads were removed as potential sequencing artifacts. We used downsampled barcode richness (number of distinct V9 rDNA barcodes) as a diversity descriptor because using V9 rDNA barcode abundances to compare plankton assemblages would likely be biased due to (i) technical limitations described in de Vargas *et al.* (*17*) and (ii) seasonality effects induced by the timing of samplings (table S1). Barcode richness was well correlated with Shannon and Simpson indexes (0.94 and 0.78, respectively). The shared barcode richness between each pair of samples (*14*) was estimated by counting, for the three larger size fractions (0.8 to 5, 20 to 180, and 180 to 2000 μm), the proportion of V9 rDNA barcodes 100% identical over their whole length. V9 rDNA barcodes were clustered into OTUs by swarm clustering as described by de Vargas *et al.* (*17*). The sub-OTU richness comparison between two samples s1 and s2 (*14*) produces three values: the number of V9 rDNA barcodes in common, the number of V9 rDNA barcodes unique to s1, and the number of V9 rDNA barcodes unique to s2. These numbers can be represented directly as bar graphs (Fig. 3B) or as dot plots of specific V9 rDNA barcode richness (Fig. 5).

Metagenomic analysis

Similarity was estimated using whole shotgun metagenomes for all four available size fractions (0.2 to 3, 0.8 to 5, 20 to 180, and 180 to 2000 μm). Because pairwise comparisons of all raw metagenome reads are intractable given the present data volume, we used a heuristic in which two metagenomic 100–base pair (bp) reads were considered similar if at least two nonoverlapping 33-bp subsequences were strictly identical (Compareads method) (*60*). For prokaryotic fractions (0.2 to 3 μm), taxonomic abundance was estimated using the number of $16S_{mi}$tags (*51*). The functional annotation, taxonomic assignation, and gene abundance estimation of the panoceanic Ocean Microbial Reference Gene Catalog (OM-RGC) (243 samples, including all those analyzed here) generated from *Tara* Oceans 0.2- to 3-μm metagenomic reads are described in Sunagawa *et al.* (*51*). Gene abundances were computed for the set of genes annotated to the nitrogen metabolism KO (*61*) group by counting the number of reads from each sample that mapped to each KO-associated gene. Abundances were normalized as reads per kilobase per million mapped reads (RPKM). Gene abundances were then aggregated (summed) for each KO group. To compare abundances between the young ring (TARA_068) and other stations, a *t* test was used. KOs with a *P* value <0.05 and a total abundance (over all stations) >10 were considered as significant (*37*). *Prochlorococcus* and *Synechococcus* community composition was analyzed in the 0.2- to 3-μm size fraction at the clade level by recruiting reads targeting the high-resolution marker gene *petB*, coding for cytochrome b_6 (*62*). The *petB* reads were first extracted from metagenomes using Basic Local Alignment Search Tool (BLASTx+) against the *petB* sequences of *Synechococcus* sp. WH8102 and *Prochlorococcus marinus* MED4. These reads were subsequently aligned against a reference data set of 270 *petB* sequences using BLASTn (with parameters set at -G 8 -E 6 -r 5 -q -4 -W 8 -e 1 -F "m L" -U T). *petB* reads exhibiting >80% identity over >90% of sequence length were then taxonomically assigned to the clade of the best BLAST hit. Read counts per clade were normalized based on the sequencing effort for each metagenomic sample. A similar approach was used with *nirA* (KO 00366) and *narB* genes (KO 00367), which were highlighted in the nitrogen-related KO analysis (Fig. 7). Phylogenetic assignment was realized at the highest possible taxonomic level using a reference data set constituted of sequences retrieved from Cyanorak v2 (www.sb-roscoff.fr/cyanorak/) and Global Ocean Sampling (*41*, *63*) databases.

Nitrogen cycle modeling

Numerical simulations of global ocean circulation were based on the Massachusetts Institute of Technology General Circulation Model (MIT-GCM) (*64*), incorporating biogeochemical and ecological components (*65*, *66*). It resolved mesoscale

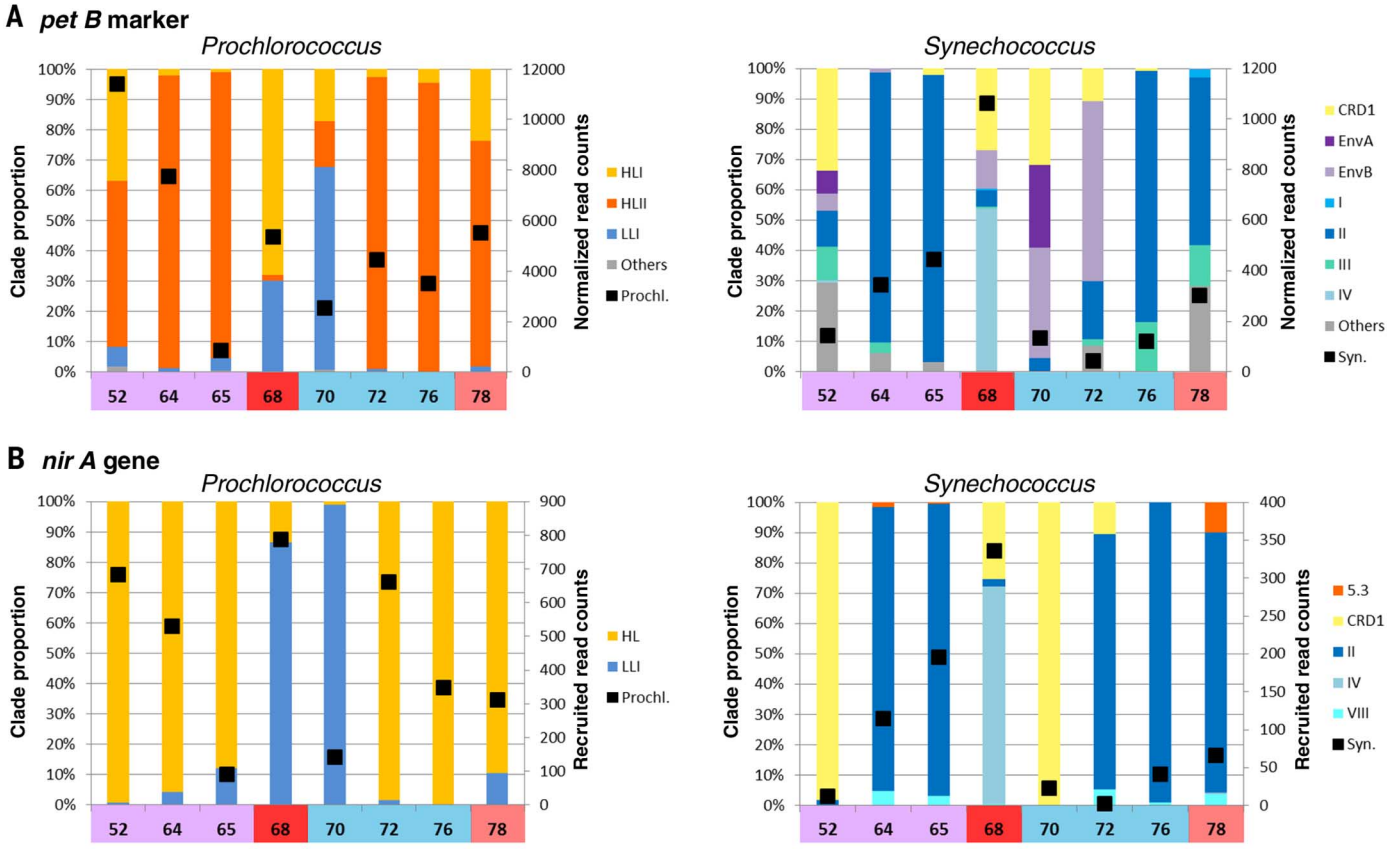

Fig. 8. Picocyanobacterial clade shift in the young Agulhas ring. (**A**) Relative abundance of *Prochlorococcus* and *Synechococcus* clades, estimated by *petB* read recruitments from 0.2- to 3-µm metagenomes. Solid squares correspond to read counts normalized based on the sequencing effort (right axis). (**B**) Relative abundance of *nirA* gene from *Prochlorococcus* and *Synechococcus* clades estimated by number of reads recruited from 0.2- to 3-µm metagenomes. The bar colors correspond to cyanobacterial clades indicated in the inset legends for each panel. Solid squares correspond to the number of reads recruited (right axis). Data are shown for stations TARA_052 to TARA_078 only, because too few cyanobacteria were found in Southern Ocean stations TARA_082, TARA_084, and TARA_085.

features in the tropics and was eddy-permitting in subpolar regions. The physical configurations were integrated from 1992 to 1999 and constrained to be consistent with observed hydrography and altimetry (*67*). Three inorganic fixed nitrogen pools were resolved—nitrate, nitrite, and ammonium—as well as particulate and dissolved detrital organic nitrogen. Phytoplankton types were able to use some or all of the fixed nitrogen pools. Aerobic respiration and remineralization by heterotrophic microbes was parameterized as a simple sequence of transformations from detrital organic nitrogen, to ammonium, then nitrification to nitrite and nitrate. In accordance with empirical evidence (*35*), nitrification was assumed to be inhibited by light. Nitrification is described in the model by simple first-order kinetics, with rates tuned to qualitatively capture the patterns of nitrogen species in the Atlantic (*66*).

Continuous spectral analysis

A continuous flow-through system equipped with a high-spectral-resolution spectrophotometer (AC-S, WET Labs, Inc.) was used for data collection during the *Tara* Oceans expedition, as described previously (*68*). Phytoplankton pigment concentrations, estimates of phytoplankton size γ, total chlorophyll a concentration, and particulate organic carbon (POC) are derived from the absorption and attenuation spectra (*69*) for the 1-km^2-binned *Tara* Oceans data set available at PANGAEA (http://doi.pangaea.de/10.1594/PANGAEA.836318).

REFERENCES AND NOTES

1. A. Biastoch, C. W. Böning, J. R. E. Lutjeharms, Agulhas leakage dynamics affects decadal variability in Atlantic overturning circulation. *Nature* **456**, 489–492http://www.ncbi.nlm.nih.gov/entrez/query.fcgi?cmd=Retrieve&db=PubMed&list_uids=19037313&dopt=Abstract (2008). doi: 10.1038/nature07426
2. A. Biastoch, C. W. Böning, F. U. Schwarzkopf, J. R. E. Lutjeharms, Increase in Agulhas leakage due to poleward shift of Southern Hemisphere westerlies. *Nature* **462**, 495–498 http://www.ncbi.nlm.nih.gov/entrez/query.fcgi?cmd=Retrieve&db=PubMed&list_uids=19940923&dopt=Abstract (2009). doi: 10.1038/nature08519
3. L. M. Beal *et al*., On the role of the Agulhas system in ocean circulation and climate. *Nature* **472**, 429–436 (2011). doi: 10.1038/nature09983; pmid: 21525925
4. F. J. C. Peeters *et al*., Vigorous exchange between the Indian and Atlantic oceans at the end of the past five glacial periods. *Nature* **430**, 661–665 (2004). doi: 10.1038/nature02785; pmid: 15295596
5. P. Cermeño, P. G. Falkowski, Controls on diatom biogeography in the ocean. *Science* **325**, 1539–1541 (2009). pmid: 19762642
6. A. L. Gordon, Oceanography: The brawniest retroflection. *Nature* **421**, 904–905 (2003). doi: 10.1038/421904a; pmid: 12606984
7. H. M. van Aken *et al*., Observations of a young Agulhas ring, Astrid, during MARE in March 20. *Deep Sea Res. Part II Top. Stud. Oceanogr.* **50**, 167–195 (2003). doi: 10.1016/S0967-0645(02)00383-1
8. J. R. Bernhardt, H. M. Leslie, Resilience to climate change in coastal marine ecosystems. *Annu. Rev. Mar. Sci.* **5**, 371–392 (2013). doi: 10.1146/annurev-marine-121211-172411; pmid: 22809195
9. E. Karsenti *et al*., A holistic approach to marine eco-systems biology. *PLOS Biol.* **9**, e1001177 (2011). doi: 10.1371/journal.pbio.1001177; pmid: 22028628
10. Companion Web site, tables W2 and W3; available at http://www.igs.cnrs-mrs.fr/Tara_Agulhas/#TablesW
11. A. H. Orsi, T. Whitworth III, W. D. Nowlin Jr., On the meridional extent and fronts of the Antarctic Circumpolar Current. *Deep-Sea Res.* **42**, 641–673 (1995). doi: 10.1016/0967-0637(95)00021-W
12. Companion Web site, tables W4 to W12; available at http://www.igs.cnrs-mrs.fr/Tara_Agulhas/#TablesW
13. Companion Web site, figure W1; available at http://www.igs.cnrs-mrs.fr/Tara_Agulhas/#FigW1
14. Companion Web site, figure W2; available at http://www.igs.cnrs-mrs.fr/Tara_Agulhas/#FigW2
15. Companion Web site, tables W13 and W14; available at http://www.igs.cnrs-mrs.fr/Tara_Agulhas/#TablesW
16. Companion Web site, figure W3; available at http://www.igs.cnrs-mrs.fr/Tara_Agulhas/#FigW3
17. C. de Vargas *et al*., Eukaryotic plankton diversity in the sunlit ocean. *Science* **348**, 1261605 (2015).
18. B. W. Bowen, L. A. Rocha, R. J. Toonen, S. A. KarlToBo Laboratory, The origins of tropical marine biodiversity. *Trends Ecol. Evol.* **28**, 359–366 (2013). doi: 10.1016/j.tree.2013.01.018; pmid: 23453048
19. R. L. Cunha *et al*., Ancient divergence in the trans-oceanic deep-sea shark *Centroscymnus crepidater*. *PLOS ONE* **7**, e49196 (2012). doi: 10.1371/journal.pone.0049196; pmid: 23145122
20. C. Schmid *et al*., Early evolution of an Agulhas Ring. *Deep Sea Res. Part II Top. Stud. Oceanogr.* **50**, 141–166 (2003). doi: 10.1016/S0967-0645(02)00382-X

21. Companion Web site, figure W4; available at http://www.igs.cnrs-mrs.fr/Tara_Agulhas/#FigW4
22. Companion Web site, figure W5; available at http://www.igs.cnrs-mrs.fr/Tara_Agulhas/#FigW5
23. Companion Web site, figure W6; available at http://www.igs.cnrs-mrs.fr/Tara_Agulhas/#FigW6
24. Companion Web site, figure W7; available at http://www.igs.cnrs-mrs.fr/Tara_Agulhas/#FigW7
25. L. Gordon, J. R. Lutjeharms, M. L. Gründlingh, Stratification and circulation at the Agulhas Retroflection. *Deep-Sea Res. A, Oceanogr. Res. Pap.* **34**, 565–599 (1987). doi: 10.1016/0198-0149(87)90006-9
26. V. Faure, M. Arhan, S. Speich, S. Gladyshev, Heat budget of the surface mixed layer south of Africa. *Ocean Dyn.* **61**, 1441–1458 (2011). doi: 10.1007/s10236-011-0444-1
27. Companion Web site, figure W8; available at http://www.igs.cnrs-mrs.fr/Tara_Agulhas/#FigW8
28. Companion Web site, figure W9; available at http://www.igs.cnrs-mrs.fr/Tara_Agulhas/#FigW9
29. Companion Web site, text W1; available at http://www.igs.cnrs-mrs.fr/Tara_Agulhas/#TextW1
30. Companion Web site, figure W10; available at http://www.igs.cnrs-mrs.fr/Tara_Agulhas/#FigW10
31. Companion Web site, figure W11; available at http://www.igs.cnrs-mrs.fr/Tara_Agulhas/#FigW11
32. Companion Web site, figure W12; available at http://www.igs.cnrs-mrs.fr/Tara_Agulhas/#FigW12
33. S. Clayton, S. Dutkiewicz, O. Jahn, M. J. Follows, Dispersal, eddies, and the diversity of marine phytoplankton. *Limnol. Oceanogr. Fluids Environ.* **3**, 182–197 (2013). doi: 10.1215/21573689-2373515
34. Companion Web site, figure W13; available at http://www.igs.cnrs-mrs.fr/Tara_Agulhas/#FigW13
35. R. J. Olson, Differential photoinhibition of marine nitrifying bacteria: A possible mechanism for the formation of the primary nitrite maximum. *J. Mar. Res.* **39**, 227–238 (1981).
36. S. Levitus *et al*., The World Ocean Database. *Data Sci. J.* **12**, WDS229–WDS234 (2013). doi: 10.2481/dsj.WDS-041
37. Companion Web site, table W15; available at http://www.igs.cnrs-mrs.fr/Tara_Agulhas/#TablesW
38. D. J. Scanlan *et al*., Ecological genomics of marine picocyanobacteria. *Microbiol. Mol. Biol. Rev.* **73**, 249–299 (2009). doi: 10.1128/MMBR.00035-08; pmid: 19487728
39. Z. I. Johnson *et al*., Niche partitioning among Prochlorococcus ecotypes along ocean-scale environmental gradients. *Science* **311**, 1737–1740 (2006). doi: 10.1126/science.1118052; pmid: 16556835
40. K. Zwirglmaier *et al*., Global phylogeography of marine Synechococcus and Prochlorococcus reveals a distinct partitioning of lineages among oceanic biomes. *Environ. Microbiol.* **10**, 147–161 (2008). pmid: 17900271
41. A. C. Martiny, S. Kathuria, P. M. Berube, Widespread metabolic potential for nitrite and nitrate assimilation among *Prochlorococcus* ecotypes. *Proc. Natl. Acad. Sci. U.S.A.* **106**, 10787–10792 (2009). doi: 10.1073/pnas.0902532106; pmid: 19549842
42. C. Hubert *et al*., A constant flux of diverse thermophilic bacteria into the cold Arctic seabed. *Science* **325**, 1541–1544 (2009). doi: 10.1126/science.1174012; pmid: 19762643
43. C. K. C. Churchill, Á. Valdés, D. Ó. Foighil, Afro-Eurasia and the Americas present barriers to gene flow for the cosmopolitan neustonic nudibranch *Glaucus atlanticus*. *Mar. Biol.* **161**, 899–910 (2014). doi: 10.1007/s00227-014-2389-7
44. N. Selje, M. Simon, T. Brinkhoff, A newly discovered *Roseobacter* cluster in temperate and polar oceans. *Nature* **427**, 445–448 (2004). doi: 10.1038/nature02272; pmid: 14749832
45. G. Casteleyn *et al*., Limits to gene flow in a cosmopolitan marine planktonic diatom. *Proc. Natl. Acad. Sci. U.S.A.* **107**, 12952–12957 (2010). doi: 10.1073/pnas.1001380107; pmid: 20615950
46. F. L. Hellweger, E. van Sebille, N. D. Fredrick, Biogeographic patterns in ocean microbes emerge in a neutral agent-based model. *Science* **345**, 1346–1349 (2014). doi: 10.1126/science.1254421; pmid: 25214628
47. D. H. Janzen, Why mountain passes are higher in the tropics. *Am. Nat.* **101**, 233–249 (1967). doi: 10.1086/282487
48. G. Wang, M. E. Dillon, Recent geographic convergence in diurnal and annual temperature cycling flattens global thermal profiles. *Nature Climate Change* **4**, 988–992 (2014). doi: 10.1038/nclimate2378
49. C. Backeberg, P. Penven, M. Rouault, Impact of intensified Indian Ocean winds on mesoscale variability in the Agulhas system. *Nature Clim. Change* **2**, 608–612 (2012). doi: 10.1038/nclimate1587
50. S. Pesant *et al*., Open science resources for the discovery and analysis of *Tara* Oceans data. http://biorxiv.org/content/early/2015/05/08/019117 (2015).
51. S. Sunagawa *et al*., Structure and function of the global ocean microbiome. *Science* **348**, 1261359 (2015).
52. J. R. Brum *et al*., Patterns and ecological drivers of ocean viral communities. *Science* **348**, 1261498 (2015).
53. J. M. Gasol, P. A. Del Giorgio, Using flow cytometry for counting natural planktonic bacteria and understanding the structure of planktonic bacterial communities. *Sci. Mar.* **64**, 197–224 (2000).
54. M. Mackey, D. Mackey, H. Higgins, S. Wright, CHEMTAX - a program for estimating class abundances from chemical markers: Application to HPLC measurements of phytoplankton. *Mar. Ecol. Prog. Ser.* **144**, 265–283 (1996). doi: 10.3354/meps144265
55. G. Gorsky *et al*., Digital zooplankton image analysis using the ZooScan integrated system. *J. Plankton Res.* **32**, 285–303 (2010). doi: 10.1093/plankt/fbp124
56. P. Hingamp *et al*., Exploring nucleo-cytoplasmic large DNA viruses in Tara Oceans microbial metagenomes. *ISME J.* **7**, 1678–1695 (2013). doi: 10.1038/ismej.2013.59; pmid: 23575371
57. Tara Oceans Consortium Coordinators; Tara Oceans Expedition, Participants (2014): Registry of selected samples from the Tara Oceans Expedition (2009-2013). doi: 10.1594/PANGAEA.840721
58. S. Chaffron, L. Guidi, F. D'Ovidio, S. Speich, S. Audic, S. De Monte, D. Iudicone, M. Picheral, S. Pesant; Tara Oceans Consortium Coordinators, Tara Oceans Expedition, Participants (2014): Contextual environmental data of selected samples from the Tara Oceans Expedition (2009-2013). doi: 10.1594/PANGAEA.840718
59. S. Chaffron, F. D'Ovidio, S. Sunagawa, S. G. Acinas, L. P. Coelho, S. De Monte, G. Salazar, S. Pesant; Tara Oceans Consortium Coordinators, Tara Oceans Expedition, Participants (2014): Contextual biodiversity data of selected samples from the Tara Oceans Expedition (2009-2013). doi: 10.1594/PANGAEA.840698
60. N. Maillet, C. Lemaitre, R. Chikhi, D. Lavenier, P. Peterlongo, Compareads: Comparing huge metagenomic experiments. *BMC Bioinformatics* **13** (suppl. 19), S10 (2012). doi: 10.1186/1471-2105-13-S19-S10; pmid: 23282463
61. M. Kanehisa *et al*., KEGG for linking genomes to life and the environment. *Nucleic Acids Res.* **36** (Database), D480–D484 (2008). doi: 10.1093/nar/gkm882; pmid: 18077471
62. S. Mazard, M. Ostrowski, F. Partensky, D. J. Scanlan, Multi-locus sequence analysis, taxonomic resolution and biogeography of marine Synechococcus. *Environ. Microbiol.* **14**, 372–386 (2012). doi: 10.1111/j.1462-2920.2011.02514.x; pmid: 21651684
63. D. B. Rusch *et al*., The Sorcerer II Global Ocean Sampling expedition: Northwest Atlantic through eastern tropical Pacific. *PLOS Biol.* **5**, e77 (2007). doi: 10.1371/journal.pbio.0050077; pmid: 17355176
64. J. Marshall, A. Adcroft, C. Hill, L. Perelman, C. Heisey, A finite-volume, incompressible Navier Stokes model for studies of the ocean on parallel computers. *J. Geophys. Res.* **102** (C3), 5753–5766 (1997). doi: 10.1029/96JC02775
65. M. J. Follows, S. Dutkiewicz, S. Grant, S. W. Chisholm, Emergent biogeography of microbial communities in a model ocean. *Science* **315**, 1843–1846 (2007). doi: 10.1126/science.1138544; pmid: 17395828
66. S. Dutkiewicz, M. J. Follows, J. G. Bragg, Modeling the coupling of ocean ecology and biogeochemistry. *Global Biogeochem. Cycles* **23**, GB4017 (2009). doi: 10.1029/2008GB003405
67. D. Menemenlis *et al*., ECCO2: High resolution global ocean and sea ice data synthesis. *Mercator Ocean Quarterly Newsletter* **31**, 13–21 (2008).
68. A. Chase *et al*., Decomposition of in situ particulate absorption spectra. *Methods in Oceanography.* **7**, 110–124 (2013). doi: 10.1016/j.mio.2014.02.002
69. E. Boss *et al*., The characteristics of particulate absorption, scattering and attenuation coefficients in the surface ocean; Contribution of the Tara Oceans expedition. *Methods in Oceanography.* **7**, 52–62 (2013). doi: 10.1016/j.mio.2013.11.002
70. K. R. Ridgway, J. R. Dunn, J. L. Wilkin, Ocean interpolation by four-dimensional least squares - Application to the waters around Australia. *J. Atmos. Ocean. Technol.* **19**, 1357–1375 (2002). doi: 10.1175/1520-0426(2002)019<1357:OIBFDW>2.0.CO;2

ACKNOWLEDGMENTS

We appreciate the commitment of the following people and sponsors: CNRS (in particular, Groupement de Recherche GDR3280); European Molecular Biology Laboratory (EMBL); Genoscope/CEA; VIB; Stazione Zoologica Anton Dohrn; UNIMIB; Fund for Scientific Research–Flanders; Rega Institute, KU Leuven; the French Ministry of Research; the French government Investissements d'Avenir programmes OCEANOMICS (ANR-11-BTBR-0008), FRANCE GENOMIQUE (ANR-10-INBS-09-08), MEMO LIFE (ANR-10-LABX-54), PSL* Research University (ANR-11-IDEX-0001-02), and ANR (projects POSEIDON/ANR-09-BLAN- 0348, PHYTBACK/ANR-2010-1709-01, PROMETHEUS/ANR-09-PCS-GENM-217, SAMOSA/ANR-13-ADAP-0010, and TARAGIRUS/ANR-09-PCS-GENM-218); European Union FP7 (MicroB3/No.287589, IHMS/HEALTH-F4-2010-261376, and MaCuMBA/No.311975); ERC Advanced Grant Award to C.B. (Diatomite: 294823); Gordon and Betty Moore Foundation grant (no. 3790) to M.B.S.; Spanish Ministry of Science and Innovation grant CGL2011-26848/BOS MicroOcean PANGENOMICS to S.G.A.; TANIT (CONES 2010-0036) from the Agència de Gestió d´Ajusts Universitaris i Reserca to S.G.A.; JSPS KAKENHI grant no. 26430184 to H.O.; NASA Ocean Biology and Biogeochemistry program (NNX11AQ14G and NNX09AU43G) to E.B.; The Italian Research for the Sea (Flagship Project RITMARE) to D.I.; and FWO, BIO5, and Biosphere 2 to M.B.S. We also appreciate the support and commitment of Agnès b. and Etienne Bourgois, the Veolia Environment Foundation, Region Bretagne, Lorient Agglomeration, World Courier, Illumina, the EDF Foundation, FRB, the Prince Albert II de Monaco Foundation, and the *Tara* schooner and its captains and crew. We thank MERCATOR-CORIOLIS and ACRI-ST for providing daily satellite data during the expedition. We are also grateful to the French Ministry of Foreign Affairs for supporting the expedition and to the countries that graciously granted sampling permissions. *Tara* Oceans would not exist without continuous support from 23 institutes (http://oceans.taraexpeditions.org). We also acknowledge excellent assistance from the European Bioinformatics Institute (EBI), in particular G. Cochrane and P. ten Hoopen, as well as the EMBL Advanced Light Microscopy Facility (ALMF), in particular R. Pepperkok. We thank Y. Timsit for stimulating scientific discussions and critical help during writing of the manuscript. The altimeter products were produced by Ssalto/Duacs and CLS, with support from CNES. The authors further declare that all data reported herein are fully and freely available from the date of publication, with no restrictions, and that all of the samples, analyses, publications, and ownership of data are free from legal entanglement or restriction of any sort by the various nations whose waters the *Tara* Oceans expedition sampled. Data described herein are available at http://www.igs.cnrs-mrs.fr/Tara_Agulhas, at EBI under the project identifiers PRJEB402 and PRJEB7988, and at PANGAEA (*57*–*59*). The data release policy regarding future public release of *Tara* Oceans data is described in Pesant *et al*. (*50*). All authors approved the final manuscript. This article is contribution number 21 of *Tara* Oceans. The supplementary materials contain additional data. See also http://doi.pangaea.de/10.1594/PANGAEA.840721; http://doi.pangaea.de/10.1594/PANGAEA.840718; and http://doi.pangaea.de/10.1594/PANGAEA.840698

Tara Oceans Coordinators

Silvia G. Acinas,[1] Peer Bork,[2] Emmanuel Boss,[3] Chris Bowler,[4] Colomban de Vargas,[5,6] Michael Follows,[7] Gabriel Gorsky,[8,9] Nigel Grimsley,[10,11] Pascal Hingamp,[12] Daniele Iudicone,[13] Olivier Jaillon,[14,15,16] Stefanie Kandels-Lewis,[2,17] Lee Karp-Boss,[3] Eric Karsenti,[4,17] Uros Krzic,[18] Fabrice Not,[5,6] Hiroyuki Ogata,[19] Stephane Pesant,[20,21] Jeroen Raes,[22,23,24] Emmanuel G. Reynaud,[25] Christian Sardet,[26,27] Mike Sieracki,[28] Sabrina Speich,[29,30] Lars Stemmann,[8] Matthew B. Sullivan,[31] Shinichi Sunagawa,[2] Didier Velayoudon,[32] Jean Weissenbach,[14,15,16] Patrick Wincker[14,15,16]

[1]Department of Marine Biology and Oceanography, Institute of Marine Science (ICM)-CSIC, Pg. Marítim de la Barceloneta, 37-49, Barcelona E08003, Spain. [2]Structural and Computational Biology, European Molecular Biology Laboratory, Meyerhofstrasse 1, 69117 Heidelberg, Germany. [3]School of Marine Sciences, University of Maine, Orono, Maine, USA. [4]Ecole Normale Supérieure, Institut de Biologie de l'ENS (IBENS), and Inserm U1024, and CNRS UMR 8197, F-75005 Paris, France. [5]CNRS, UMR 7144, Station Biologique de Roscoff, Place Georges Teissier, 29680 Roscoff, France. [6]Sorbonne Universités, UPMC Univ Paris 06, UMR 7144, Station Biologique de Roscoff, Place Georges Teissier, 29680 Roscoff, France. [7]Department of Earth, Atmospheric and Planetary Sciences, Massachusetts Institute of Technology, Cambridge, MA, USA. [8]CNRS, UMR 7093, LOV, Observatoire Océanologique, F-06230 Villefranche-sur-Mer, France. [9]Sorbonne Universités, UPMC Univ Paris 06, UMR 7093, LOV, Observatoire Océanologique, F-06230 Villefranche-sur-Mer, France. [10]CNRS UMR 7232, BIOM, Avenue du Fontaulé, 66650 Banyuls-sur-Mer, France. [11]Sorbonne Universités

Paris 06, OOB UPMC, Avenue du Fontaulé, 66650 Banyuls-sur-Mer, France. [12]Aix Marseille Université CNRS IGS UMR 7256, 13288 Marseille, France. [13]Stazione Zoologica Anton Dohrn, Villa Comunale, 80121 Naples, Italy. [14]CEA, Institut de Génomique, GENOSCOPE, 2 rue Gaston Crémieux, 91057 Evry, France. [15]CNRS, UMR 8030, CP5706, Evry, France. [16]Université d'Evry, UMR 8030, CP5706, Evry, France. [17]Directors' Research, European Molecular Biology Laboratory, Heidelberg, Germany. [18]Cell Biology and Biophysics, European Molecular Biology Laboratory, Meyerhofstrasse 1, 69117 Heidelberg, Germany. [19]Institute for Chemical Research, Kyoto University, Gokasho, Uji, Kyoto, 611-0011, Japan. [20]PANGAEA, Data Publisher for Earth and Environmental Science, University of Bremen, Bremen, Germany. [21]MARUM, Center for Marine Environmental Sciences, University of Bremen, Bremen, Germany. [22]Department of Microbiology and Immunology, Rega Institute, KU Leuven, Herestraat 49, 3000 Leuven, Belgium. [23]Center for the Biology of Disease, VIB, Herestraat 49, 3000 Leuven, Belgium. [24]Department of Applied Biological Sciences, Vrije Universiteit Brussel, Pleinlaan 2, 1050 Brussels, Belgium. [25]Earth Institute, University College Dublin, Dublin, Ireland. [26]CNRS, UMR 7009 Biodev, Observatoire Océanologique, F-06230 Villefranche-sur-Mer, France. [27]Sorbonne Universités, UPMC Univ Paris 06, UMR 7009 Biodev, F-06230 Observatoire Océanologique, Villefranche-sur-Mer, France. [28]Bigelow Laboratory for Ocean Sciences, East Boothbay, USA. [29]Department of Geosciences, Laboratoire de Météorologie Dynamique (LMD), Ecole Normale Supérieure, 24 rue Lhomond 75231 Paris Cedex 05, France. [30]Laboratoire de Physique des Océans, UBO-IUEM, Place Copernic, 29820 Plouzané, France. [31]Department of Ecology and Evolutionary Biology, University of Arizona, 1007 East Lowell Street, Tucson, AZ 85721, USA. [32]DVIP Consulting, Sèvres, France.

SUPPLEMENTARY MATERIALS

www.sciencemag.org/content/348/6237/1261447/suppl/DC1
Table S1

18 September 2014; accepted 23 February 2015
10.1126/science.1261447

Science
AAAS

Environmental characteristics of Agulhas rings affect interocean plankton transport

Emilie Villar *et al.*

Science **348**, (2015);
DOI: 10.1126/science.1261447